NANO LETTERS

2008
Vol. 8, No. 2
565−570

Structural Coherency of Graphene on Ir(111)

Johann Coraux,* Alpha T. N′Diaye, Carsten Busse, and Thomas Michely

II. Physikalisches Institut, Universität zu Köln, Zülpicher Str. 77, 50937 Köln, Germany

Received November 5, 2007

ABSTRACT

Low-pressure chemical vapor deposition allows one to grow high structural quality monolayer graphene on Ir(111). Using scanning tunneling microscopy, we show that graphene prepared this way exhibits remarkably large-scale continuity of its carbon rows over terraces and step edges. The graphene layer contains only a very low density of defects. These are zero-dimensional defects, edge dislocation cores consisting of heptagon–pentagon pairs of carbon atom rings, which we relate to small-angle in-plane tilt boundaries in the graphene. We quantitatively examined the bending of graphene across Ir step edges. The corresponding radius of curvature compares to typical radii of thin single-wall carbon nanotubes.

Graphene is the name given to a single monolayer of graphite. It provided the first macroscopic and experimental evidence of quantum charge carriers exhibiting relativistic behavior, together with new physical phenomena such as half integer quantum Hall effect,[1,2] quantization of electrical resistivity,[1] or weak antilocalisation.[3] Being an atomically thin half-metal, graphene also is a potential building block for future nanoelectronics, as it allows electric field-effect with giant room-temperature mobility of charge carriers.[4] Recently, it was nanopatterned using conventional lithography methods with maintained structural quality, such that quantum confinement and quantum interferences in nanosized graphene could now be utilized for unconventional nanoelectronics.[5]

Along the view of designing graphene-based nanoelectronic devices, the achievement of large scale graphene in a reproducible way with controlled structural quality and on the desired support is of major importance and remains a major stake. It is also of prior fundamental significance to further address the exceptional relativistic quantum electronic properties of such graphene layers, independent from the contribution of structural defects. Such defects are point defects that influence the transport properties through quantum interferences[6,7] or defects induced by the underlying substrate, like surface irregularities[7] or step edges. Noteworthy, point defects may play a constructive role in tuning graphene's physical properties, as they should promote magnetism[8] or even the unconventional quantum Hall effect.[3] If desired, such defects could be introduced in a controlled manner into high structural quality graphene using, for example, electron irradiation.[9]

Various growth methods are currently used to prepare graphene. Mechanical exfoliation of graphite allows for micrometer scale graphene layers to be obtained either on amorphous substrates such as silicon oxide[4] or in a free-standing form.[10] Though it provides with large scale graphene sheets, such a method is not adapted to the implementation in hypothetical devices, as underlined by Geim and Novoselov.[11] Epitaxial graphene is on the contrary more suited to this respect. Such graphene mono-, bi-, tri-, etc, layers can be grown on silicon carbide (SiC) substrates out of successive annealing sequences of a Si-rich SiC(0001) surface[12] leading to micrometer scale extension of graphene, which was proposed to continuously cross step edges.[13] However, to the best of our knowledge this method induces noticeable densities of defects.[7] Graphene monolayers can also be prepared on metallic surfaces, most often through thermal decomposition of hydrocarbons or surface segregation of C atoms from the bulk metal. Accordingly, graphene was synthesized onto Co(0001),[14] Ni(111),[15] Pt(111),[16−18] Pd(111),[19] Ru(0001),[20] or Ir(111).[21−23] For small lattice mismatches below 1%, commensurate superstructures are formed, as it is the case for Co(0001)[14] and Ni(111).[15] In contrast, larger mismatches can yield incommensurate moiré superstructures, for instance, on Pt(111),[16] Ir(111),[22] or Ru(0001).[20] Graphene prepared on Ir(111) via adsorption and subsequent thermal decomposition of ethylene at appropriate temperature yields flakes of well-defined orientation.[22] On the contrary, graphene obtained via thermal decomposition of ethylene on Pt(111) or high-temperature segregation of C on Ru(0001) displays a spread of orientations. Graphene layers on metal surfaces could possibly be transferred to other supports following overgrowth of, for example, an oxide layer and subsequent chemical etching of the underlying

* Corresponding author. Phone: +49-221-470-2751. Fax: +49-221-470-5178. E-mail: coraux@ph2.uni-koeln.de..

10.1021/nl0728874 CCC: $40.75
Published on Web 01/12/2008

metallic substrate, opening the way to nanoelectronic build-up.[11] Noticeably, moirés can be used as templates for the self-organized growth of metallic nanoclusters, as recently evidenced by Ir nanocluster growth on graphene/Ir(111).[22] Such nanocluster arrays have potential for nanomagnetism and nanocatalysis.

In this letter, we focus on graphene monolayers grown by low-pressure chemical vapor deposition (CVD) of ethylene on the hot Ir(111) surface. Compared to previous work related to graphene flakes achieved by pyrolysis of pread-sorbed ethylene at high temperatures,[22] CVD grown graphene may fully cover the Ir(111) surface if prepared under appropriate conditions. The epitaxial relation of $\langle 10\bar{1}\rangle_{Ir}$ Ir rows and $\langle 11\bar{2}0\rangle_{C}$ C rows being parallel is satisfied at high growth temperatures to high perfection at 1320 K, while at lower temperature (e.g., 1120 K) a few degrees of scatter are present. Thorough description of the growth method and extensive comparison between the two preparation methods are beyond the scope of the present article and will be addressed elsewhere.

The aim of the present contribution is to describe and understand graphene's structural coherency occurring over micrometer distances. We first address the continuity of the C rows on terraces and relate the presence of moiré domains to small-angle in-plane one-dimensional tilt boundaries. Next, we analyze the coherency between terraces and its correlation to graphene bending over step edges. For these purposes, we take benefit of the moiré superstructure of graphene on Ir(111) as a magnifying lens unraveling sub-ångström atomic displacements and sub-degree misorientations. Real space imaging down to the atomic scale provides direct and complementary evidence of the C row continuity and of the structure of atomic defects.

Experiments were performed in an ultrahigh vacuum chamber with low 10^{-10} mbar base pressure using a variable temperature scanning tunneling microscope (STM). The substrate's surface was prepared by several cycles consisting of sputtering at 1120 K by a 1.5 keV mass separated Xe^+ ion beam and flash annealing at 1520 K. Graphene was grown through ethylene CVD at 1120, 1220, or 1320 K.

Figure 1a is an STM topograph of a region of a graphene sheet grown at 1120 K (1 L of ethylene), where two step edges are visible. The observed in-plane periodicity of about 2.5 nm is that of the moiré superstructure with each dark spot corresponding to an "on-top" like region where C rings tend to have their center above an Ir atom.[22,24] Two rows of defects are visible in Figure 1a. They lie at the border of three moiré domains, defined by the orientation of their moiré. These observations are summarized in Figure 1b, where one additionally notices that the orientation of the moiré remains the same across a step edge. From the angle $\Delta\theta_m$ of misorientation between hexagonal patterns of two moiré domains (Figure 1b), we derive the angle $\Delta\theta_{at}$ of the corresponding misorientation of the atomic C rows in the domains. Let $\vec{\mathbf{k}}_{C,1}$, $\vec{\mathbf{k}}_{C,2}$, and $\vec{\mathbf{k}}_{Ir}$ be the reciprocal space vectors corresponding to the $1/\sqrt{6}[11\bar{2}0]_{C,1}$, $1/\sqrt{6}[11\bar{2}0]_{C,2}$ unit vectors of the C lattices in domains (1, 2)[25] and to the $1/2[10\bar{1}]_{Ir}$ unit vector of the Ir lattice lying in the (111)

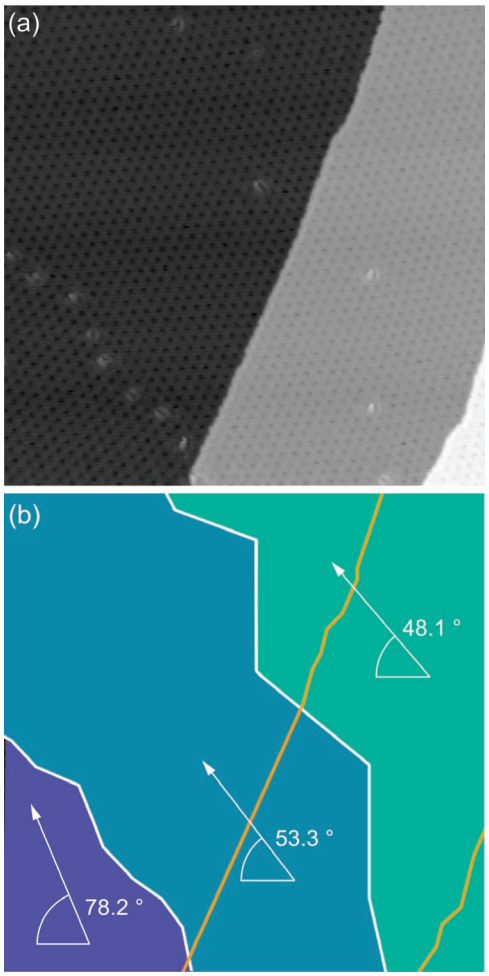

Figure 1. (a) 108 nm × 108 nm STM topograph (−0.05 V, 30 nA) of a graphene monolayer grown on Ir(111) at 1120 K, exhibiting two step edges and three moiré domains with different orientations of their moiré. (b) Corresponding map of domains and orientations.

surface. $k_{Ir} = 1/a_{Ir} = (1/0.2715)$ nm^{-1} and $k_{C,1} = k_{C,2} = k_C = 1/a_C = (1/0.2452)$ nm^{-1} for graphene on Ir(111).[24] One obtains the corresponding reciprocal space vector associated with the moiré patterns in domains (1, 2) by $\vec{\mathbf{k}}_{m,i} = \vec{\mathbf{k}}_{C,i} - \vec{\mathbf{k}}_{Ir}$, with $i = 1,2$. Since $\vec{\mathbf{k}}_{m,2} - \vec{\mathbf{k}}_{m,1} = \vec{\mathbf{k}}_{C,2} - \vec{\mathbf{k}}_{C,1}$, one may easily show that $\sin(\Delta\theta_{at}/2) = \sqrt{k_{m,1}^2 + k_{m,2}^2 - 2k_{m,1}k_{m,2}\cos(\Delta\theta_m)}/(2k_C)$, which yields $\Delta\theta_{at} = (2.31 \pm 0.15)°$ [$\Delta\theta_{at} = (0.48 \pm 0.07)°$] between the lower [upper] domains in Figure 1, while the moiré periodicity varies by roughly 4% from the bottom to the top domain in the image.

Understanding the accommodation of such small-angle misorientations was achieved by atomic scale characterization of the defects occurring at the boundaries. Figure 2a is an STM topograph at atomic scale of one of these defects (similar to those observed in Figure 1a). Dark spots correspond to the centers of the C rings.[22,24] Figure 2b shows a larger view of the defect, together with the orientation of the two moirés around it. In Figure 2c, the centers of C rings were located by triangulation. The network of lines connecting C ring centers unambiguously shows two extra lines that start at the location of the bright protrusion. The two

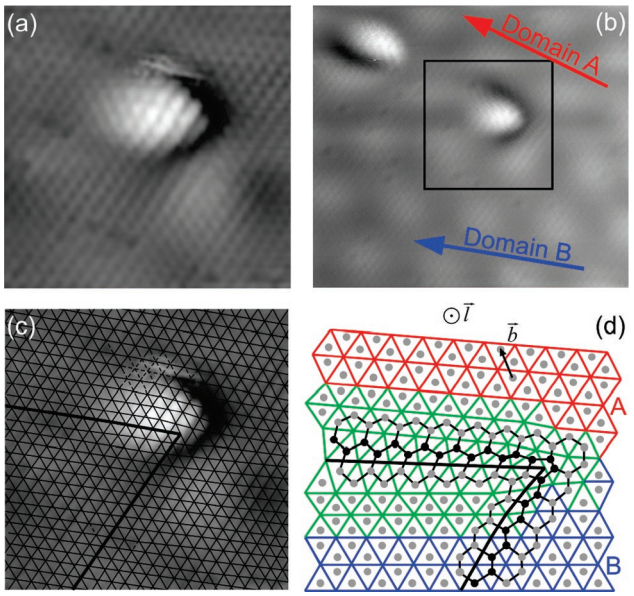

Figure 2. (a) Atomic resolution 5.5 nm × 5.5 nm STM topograph (Fourier filtered, 0.1 V, 9 nA) of a graphene layer grown on Ir-(111) at 1120 K. (b) Demagnified view (14 nm × 12.4 nm) showing two defects at the boundary between two moiré domains (A, B); the area within the black frame is panel a demagnified. (c) Line network connecting the centers of the C rings in panel a. In regions where the contrast is lost, the atomic arrangement was extrapolated (dashed lines). Thick solid lines indicate the presence of extra lines. (d) Scheme of the correspondence between the network in panel c and the C atoms in the vicinity of the wedge, lying at the tilt boundary between domain A and B shown in panel b. A and B are misoriented by a rotation along the $\vec{\mathbf{l}}$ normal to the surface. Two extra atomic rows corresponding to an edge dislocation with Burger's vector $\vec{\mathbf{b}}$ ($b = a_C = 0.2452$ nm) are outlined (black circles). Note the relative orientation of the wedge and of the C pentagon and heptagon.

extra lines correspond to two extra C rows, that is, a single edge dislocation in a hexagonal lattice. This is sketched in Figure 2d, where the line network is related to the atomic arrangement. One observes two extra C zigzag rows along $\langle 11\bar{2}0\rangle_C$ crystallographic directions of the C lattice (graphene) corresponding to a Burger's vector $\vec{\mathbf{b}} = 1/\sqrt{6}\langle 11\bar{2}0\rangle_C$. The protrusion-like feature observed in Figure 2, panels a and b, in the vicinity of the dislocation could well be caused by electron scattering from the structural defect[6,7] or by a moiré-like contrast originating from the atomic displacements induced at the dislocation core.

Edge dislocations are well known to efficiently accommodate small-angle misorientations between crystallites.[26] To check whether this is actually the driving force for creation of edge dislocations in graphene on Ir(111), we evaluated the misorientation between C rows in the two neighboring domains of Figure 2. As explained above, this can be accurately determined taking benefit of the moiré effect. We find $\Delta\theta_{at} = (2.07 \pm 0.12)°$, that is, a small-angle misorientation. The projection $\vec{\mathbf{r}}$ of the vector joining two dislocations onto the tilt boundary, which direction is the bisecting line between the vectors defining the orientation of the misoriented moirés, is related to the dislocations Burger's vector $\vec{\mathbf{b}}$ ($b = a_C = 0.2452$ nm in the case of Figure 2) and to $\Delta\theta_{at}$ by Frank's formula:[26] $\vec{\mathbf{b}} = \vec{\mathbf{r}} \times \vec{\mathbf{l}} \cdot 2 \sin(\Delta\theta_{at}/2)$, where $\vec{\mathbf{l}}$ is the normal to the tilted domains, that is, the normal to graphene's surface (see Figure 2d). This leads to $r = (6.8 \pm 0.4)$ nm, which is in good agreement with the projection of the distance between the edge dislocations visible in Figure 2b as bright protrusions, onto the tilt boundary [(6.2 ± 1.3) nm]. As an additional illustration, the misorientations observed in Figure 1 should yield $r = (6.1 \pm 0.4)$ nm and $r = (29.3 \pm 4.3)$ nm for the two defect lines, which is in reasonable agreement with the actual projection of the separation of bright protrusions visible on the STM image, onto the tilt boundary [(8.3 ± 1.5) nm and (26.7 ± 5.0) nm, respectively].

Figure 2c reveals in a quite direct way the atomic structure of the edge dislocation, which is a zero-dimensional defect in the two-dimensional (2D) crystal of graphene. The edge dislocation actually consists of one C pentagon of which the center is the end of the wedge shown in Figure 2, panels c and d, together with one C heptagon adjacent to the pentagon and located along the bisecting line between the two directions composing the wedge. Several atomic scale STM images (not shown) with moiré domain boundaries were analyzed using the procedure described above. We always find at the position of the bright protrusions an edge dislocation and a heptagon−pentagon pair. Edge dislocations in 2D crystals were evidenced years ago in dense-packed planar lattices of soap bubbles.[27] They were more recently identified in noble gas layers on graphite and related to the discommensuration of the noble gas domains, using STM.[28] In C materials, heptagon−pentagon pairs were first considered in C_{60} molecules as potential elements of the molecule[29] and later ruled out. They were also speculated to exist in graphite at the boundary between misoriented domains but could not be resolved in the STM images.[30] The occurrence of such pairs was even proposed in irradiated graphene and carbon nanotubes by extrapolating high-resolution transmission electron microscopy (HR-TEM) images by simulations. Because of lack of spatial resolution, HR-TEM itself could not provide the details of the atomic arrangement.[9] Our atomic scale results complement these former studies with a direct evidence for heptagon−pentagon pairs in graphene.

Considering the spatial extension of graphene raises the question whether there is structural coherency, that is, continuation of C rows, across Ir step edges or not. We observe moiré domains extending across Ir(111) step edges at 1120 (see Figure 1a) and 1220 K. Increasing the growth temperature to 1320 K results in moiré domains of micrometer size extending over numerous step edges. For such large moiré domains as shown in Figure 3a, the $\langle 11\bar{2}0\rangle_C$ direction of C rows in graphene is accurately parallel to the Ir surface dense-packed $\langle 10\bar{1}\rangle_{Ir}$ direction, and no edge dislocation is found throughout micrometer distances. Figure 3b is an STM topograph of graphene grown at 1120 K where all C rows are observed to be continuous across a step, that is, graphene lies like a blanket over the step edge, which is a typical situation. Occasionally, situations arise where most of the C rows are continuous over step edges, but a small fraction of C rows that stop at step edges (2D edge dislocations) to accommodate the complex bending of graphene (not shown)

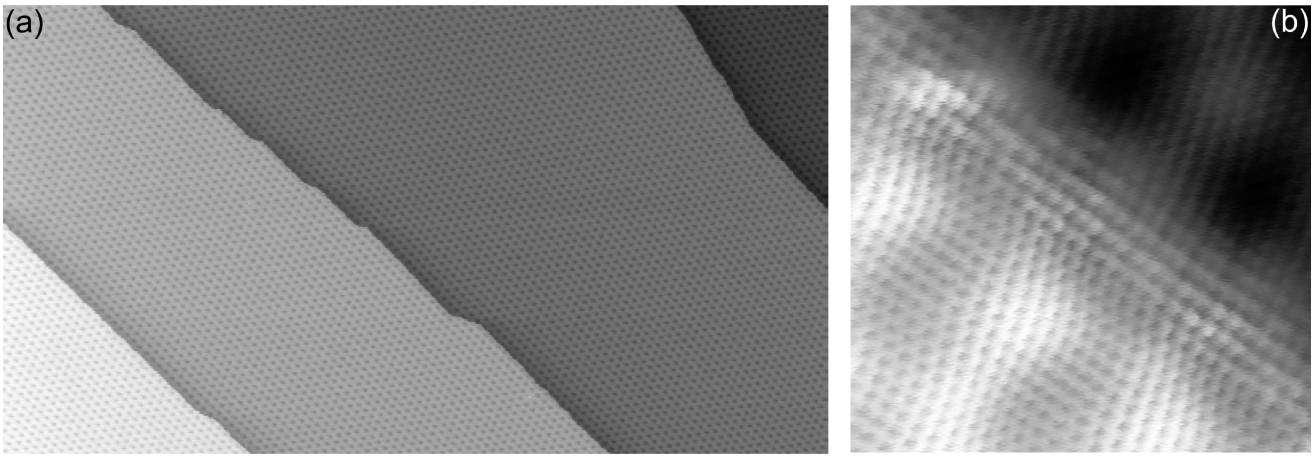

Figure 3. (a) 125 nm × 250 nm STM topograph (0.10 V, 30 nA) of graphene grown on Ir(111) at 1320 K, crossing several Ir steps. (b) Continuous atomic arrangement in graphene across a step edge (5 nm × 5 nm, 0.04 V, 30 nA).

were observed. The picture of structural coherency of graphene over step edges is also supported by sets of STM snapshots of the Ir(111) surface exposed to increasing amounts of ethylene at 1120 K. It was accordingly found that graphene growth starts from islands nucleated at step edges and proceeds to both sides of the step edge.

The structural coherency of graphene across steps as evidenced above by atomically resolved images should also be reflected in the alignment of the moiré patterns on the neighboring terraces. It should be noted that the moiré structure shows very high sensitivity toward faint atomic displacements. For example, a shift of graphene parallel to the Ir $[10\bar{1}]_{Ir}$ direction by one nearest neighbor distance (a_C = 0.2715 nm) causes a parallel shift of the moiré lattice by a full moiré period (≈2.5 nm). As shown in Figures 1a and 3b, we typically observe the same orientation and periodicity of moiré patterns on the upper and lower side of the step, which is a necessary condition for structural coherency across steps. For the description of the relative alignment, we will focus in the following for simplicity on the dense-packed Ir steps edges along $\langle 10\bar{1}\rangle_{Ir}$ of either {111} (B-steps) or {100} (A-steps) microfacets. We find that lines joining brightness minima of the moiré structure (on-top type areas) in the $\langle 1\bar{1}00\rangle_C$ direction (see Figure 4a) exhibit no sideward shift when crossing an Ir step within an uncertainty of 10% of the moiré periodicity perpendicular to the step (≈4.3 nm). To account for this observation, we developed an elementary model of graphene bending at the step edge, as shown in Figure 4a, where one observes that the moiré brightness maxima (imaged as minima on the STM images) on both terraces are located along the same line parallel to $\langle 1\bar{1}00\rangle_C$.[31] Noteworthy, this behavior was also present, though not described, for graphene on Ru(0001), as can be seen on several STM images (Figure 2a in ref 32 and Figure 4b in ref 20).

The bending of the graphene at a step edge necessarily induces a Δ_C shift in the graphene structure along the $\langle 1\bar{1}00\rangle_C$ direction (i.e., perpendicular to the step edges) with respect to a hypothetical unbent graphene (see Figure 4c). This shift should cause a Δ_m shift of the moiré lattices from a terrace to the other, along the opposite direction. Such a shift is evaluated in Figure 4d, which shows a line profile along such a direction, where each minimun corresponds to a moiré brightness minimum. The periodic profiles and therefore the moiré sites on both sides of the step edge are dephased by Δ_m perpendicular to the step edge. For A-steps, a systematic analysis over several step edges reveals a typical Δ_m shift corresponding to +50% with 10% dispersion of the repeat distance in the moiré lattice along $\langle 1\bar{1}00\rangle_C$, that is, +2.19 nm with 0.44 nm dispersion. For B-steps, a similar analysis yields $\Delta_m = -0.77$ nm with 0.44 nm dispersion. Part of this shift is intrinsic to the Ir(111) terraces, namely Ir atoms are laterally shifted (Δ_{Ir}) from a terrace to the other according to the fcc stacking (see Figure 4d). For an A-step (B-step) $\Delta_{Ir} = +\sqrt{3}a_{Ir}/3 = +0.1568$ nm ($\Delta_{Ir} = -\sqrt{3}a_{Ir}/3 = -0.1568$ nm). The Δ_m shift was then translated in terms of an atomic shift Δ_C, through $k_C'\Delta_C = k_{Ir}'\Delta_{Ir} - k_m'\Delta_m$, where $k_C' = 1/(\sqrt{3}a_C) = (1/0.425)$ nm^{-1} and $k_{Ir}' = 1/(\sqrt{3}a_{Ir}) = (1/0.470)$ nm^{-1} correspond to reciprocal space vectors $\vec{\mathbf{k}}_C'$ and $\vec{\mathbf{k}}_{Ir}'$ perpendicular to the previously defined $\vec{\mathbf{k}}_C$ and $\vec{\mathbf{k}}_{Ir}$ vectors, and k_m' corresponds to the moiré reciprocal space vector, $\vec{\mathbf{k}}_m' = \vec{\mathbf{k}}_C' - \vec{\mathbf{k}}_{Ir}'$, which is perpendicular to the previously defined $\vec{\mathbf{k}}_m$ vector. This yields $\Delta_C = -0.073$ nm with 0.022 nm dispersion for A-steps dispersion, and $\Delta_C = -0.067$ nm with 0.030 nm dispersion for B-steps.

The last step was to relate this atomic shift to the bending of the graphene. For that purpose, we developed an elementary model depicted in Figure 4c. Within that model the graphene layer across the step edge was approximated by two identical arcs of cylinders with radius R, and arc angle θ. We fixed continuous conditions on both the graphene sheet and its derivative and imposed a constant graphene height before the step edge and well after. Two relationships are needed to extract both R and θ from Δ_C. The first one is set by the boundary conditions, namely the projection of one arc of circle onto the out-of-plane direction equals half an Ir step edge height (s), $s/2 = R(1 - \cos\theta)$. The second relationship is the definition of the atomic shift, which is the difference between the arc length and its projection onto the flat surface, modulus an integer number (n) of C rings: $\Delta_C = -(2R\theta - 2R\sin\theta) + nd_{CC}$ with d_{CC} being the C period along the bending direction and $d_{CC} = 1/k_C' = 0.425$ nm in

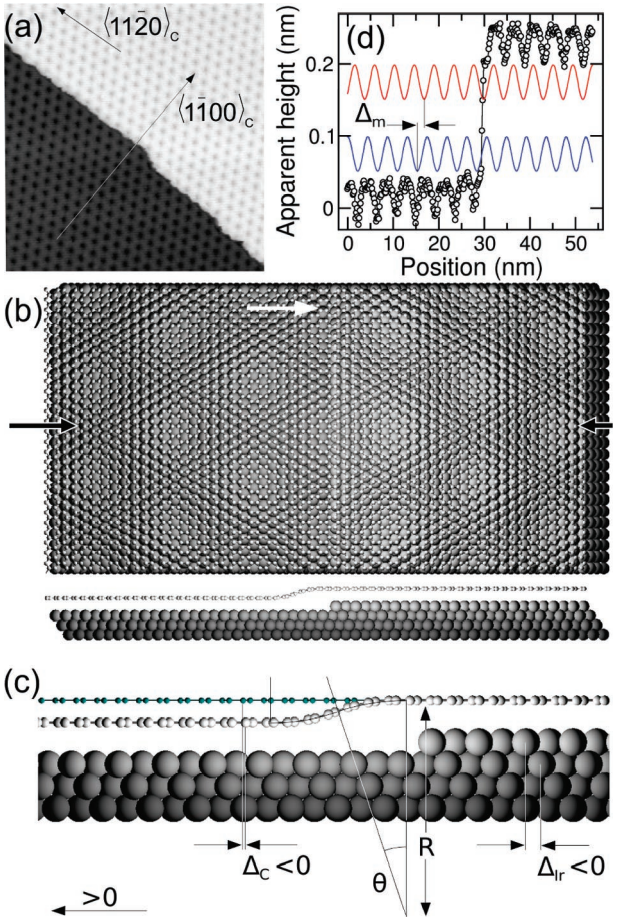

Figure 4. (a) 60 nm × 60 nm STM topograph (0.11 V, 30nA) of a single moiré domain grown at 1320 K. Undisturbed by the visible B-step, the moiré minima along the $\langle 1\bar{1}00\rangle_C$ direction are centered on a straight line. (b) Ball-model top and side views of a graphene sheet crossing an Ir B-step edge. The incommensurate Ir(111) surface lattice and graphene are superimposed in the experimentally observed orientation with $\langle 1\bar{1}00\rangle_C$ (white arrow) parallel to the $\langle \bar{1}\bar{1}2\rangle_{Ir}$ direction of Ir. The moiré brightness maxima in the ball-model along $\langle 1\bar{1}00\rangle_C$ are centered on a straight line extending over the step edge (in between the two black arrows). Note that the ball-model brightness maxima are imaged as brightness minima by STM. The moirés on the two terraces are shifted perpendicular to the step edge (Δ_m). (c) Close up side view of the Ir B-step edge and graphene sheet crossing it. The curvature is modeled by two identical arcs of cylinders (R, θ) with continuous boundary conditions at all junctions. The C atoms shift (Δ_C) with respect to hypothetical unbent graphene (small green circles) is related to the moiré shift Δ_m and the shift (Δ_{Ir}) between Ir atoms from a terrace to the other (see text for details). (d) Apparent height along the $\langle 1\bar{1}00\rangle_C$ direction of the graphene lattice, shown in panel a.

the present case. Provided that Δ_C may only vary between 0 nm (unbent graphene) and the step height, $s = \sqrt{2/3}a_{Ir} = 0.222$ nm, and because $s < d_{CC}$, n must be equal to 0. The system of nonlinear equations with R and θ as unknowns is then solved numerically for each value of Δ_C. R is found to have an average of 0.27 nm with an asymmetric dispersion of 0.10 and 0.25 nm toward lower and higher values, respectively. The asymmetry arises from the nonlinearity of the system of equations to be solved, which conveys into increased dependence of R upon small changes of Δ_C when Δ_C decreases. The value of 0.27 nm is small and corresponds to radii of very thin single wall carbon nanotubes.[33]

In summary, graphene monolayers grown by low-pressure CVD of ethylene on hot Ir(111) are fully coherent over step edges on scales larger than micrometers. Graphene lies like a blanket on the substrate and bends over step edges with radii of curvature similar to those of thin single wall carbon nanotubes. The only defects we found in the graphene lattice are edge dislocations forming pentagon−heptagon carbon atom rings. These edge dislocations are spread in low density and with characteristic separation to form small angle tilt boundaries in the graphene lattice. They also may occasionally be found at step edges. The observation of moiré domains amplifies strongly the small orientation differences of the graphene lattice but does not imply a structural disintegrity of graphene. At sufficiently high growth temperatures, the moiré domains reach at least micrometer sizes thereby minimizing the concentration of edge dislocations in the lattice.

Our results are likely of interest for achieving large-sized, high structural quality epitaxial graphene sheets. The transport properties of graphene as a function of the density and the electronic properties of defects, as well as the use of such large graphene sheets for subsequent self-organized growth of magnetic or catalytic nanoclusters, are meaningful examples encouraging further research on graphene/metal materials.

Acknowledgment. J.C. thanks the Alexander von Humboldt foundation for a research fellowship. Financial support through the DFG research grant "Two Dimensional Cluster Lattices on Graphene Moiré on Dense-Packed Metal Surfaces" is acknowledged.

References

(1) Novoselov, K. S.; Geim, A. K.; Morosov, S. V.; Jiang, D.; Katsnelson, M. I.; Grigorieva, I. V.; Dubonos, I. V.; Firsov, A. A. *Nature* **2005**, *438*, 197.
(2) Zhang, Y.; Tan, Y.-W.; Stormer, H. L.; Kim, P. *Nature* **2005**, *438*, 201.
(3) Wu, X.; Li, X.; Song, Z.; Berger, C.; de Heer, W. A. *Phys. Rev. Lett.* **2007**, *98*, 136801.
(4) Novoselov, K. S.; Geim, A. K.; Morozov, S. V.; Jiang, D.; Zhang, Y.; Dubonos, S. V.; Grigorieva, I. V.; Firsov, A. A. *Science* **2004**, *306*, 666.
(5) Berger, C.; Song, Z.; Li, X.; Wu, X.; Brown, N.; Naud, C.; Mayou, D.; Li, T.; Hass, J.; Marchenkov, A. N.; Conrad, E. H.; First, P. N.; de Heer, W. A. *Science* **2006**, *312*, 1191.
(6) Mallet, P.; Farchone, V.; Magaud, L.; Berger, C.; Veuillen, J.-Y. *Phys. Rev B* **2007**, *76*, R041403.
(7) Rutter, G. M.; Crain, J. N.; Guisinger, N. P.; Li, T.; First, P. N.; Stroscio, J. A. *Science* **2007**, *317*, 219.
(8) Lehtinen, P. O.; Foster, A. S.; Ayuela, A.; Krasheninnikov, A.; Nordlund, K.; Nieminen, R. M. *Phys. Rev. Lett.* **2003**, *91*, 017202.
(9) Hashimoto, A.; Suenega, K.; Gloter, A.; Urita, K.; Lijima, S. *Nature* **2004**, *430*, 870.
(10) Meyer, J. C.; Geim, A. K.; Katsnelson, M. I.; Novoselov, K. S.; Booth, T. J.; Roth, S. *Nature* **2007**, *416*, 40.
(11) Geim, N. K.; Novoselov, K. S. *Nat. Mater.* **2007**, *6*, 183.
(12) Forbeaux, I.; Themlin, J.-M.; Debever, J.-M. *Phys. Rev. B* **1998**, *58*, 16396.
(13) Berger, C.; Song, Z.; Li. T.; Li, X.; Ogbazghi, A. Y.; Fenr. R.; Dai, Z.; Marchenkov, A. N.; Conrad, E. H.; First, P. N.; de Heer, W. A. *J. Phys. Chem.* **2004**, *108*, 19912.
(14) Vaari, J.; Lahtinen, J.; Hautojärvi, P. *Catal. Lett.* **1997**, *44*, 43.
(15) Gamo, Y.; Nagashima, A.; Wakabayashi, M.; Terai, M.; Oshima, C. *Surf. Sci.* **1997**, *374*, 61.
(16) Land, T. A.; Michely, T.; Behm, R. J.; Hemminger, J. C.; Comsa, G. *Surf. Sci.* **1992**, *264*, 261.

(17) Ueta, H.; Saida, M.; Nakai, C.; Yamada, Y.; Sasaki, M.; Yamamoto, S. *Surf. Sci.* **2004**, *560*, 183.
(18) Starr, D. E.; Pazhetnov, E. M.; Stadnichenko, A. I.; Boronin, A. I.; Shaikhutdinov, S. K. *Surf. Sci.* **2006**, *600*, 2688.
(19) Oshima, J.; Nagashima, A. *J. Phys.: Condens. Matter* **1997**, *9*, 1.
(20) Marchini, S.; Günther, S.; Wintterlin, J. *Phys. Rev. B* **2007**, *76*, 075429.
(21) Gall', N. R.; Rut'kov, E. V.; Tontegode, A. Y. *Phys. Solid State* **2004**, *46*, 371.
(22) N′Diaye, A. T.; Bleikamp, S.; Feibelman, P.; Michely, T. *Phys. Rev. Lett.* **2006**, *97*, 215501.
(23) Makarenko, I. V.; Titkov, A. N.; Waqar, Z.; Dumas, P.; Rutkov, E. V.; Gall, N. R. *Phys. Solid State* **2007**, *49*, 371.
(24) N′Diaye, A. T.; Coraux, J.; Plasa, T. N.; Busse, C.; Michely, T. To be published.
(25) Frank, F. C. *Acta Crystallogr.* **1964**, *18*, 862.
(26) Bollmann, W. *Discuss. Faraday Soc.* **1964**, *38*, 26.
(27) Bragg, W. L.; Nye, J. F. *Proc. R. Soc. London* **1947**, *A190*, 474.
(28) Grimm, B.; Hövel, H.; Bödecker, M.; Fieger, K.; Reihl, B. *Surf. Sci.* **2000**, *454*, 618.
(29) Stone, A. J.; Wales, D. J. *Chem. Phys. Lett.* **1986**, *128*, 501.
(30) Simonis, P.; Goffaux, C.; Thiry, P. A.; Biro, L. P.; Lambin, P.; Meunier, V. *Surf. Sci.* **2002**, *511*, 319.
(31) Strictly speaking, continuity of lines joining brightness maxima of the moiré along $\langle 1\bar{1}00\rangle_C$ implies that both lines joining carbon atoms along $\langle 1\bar{1}00\rangle_C$ in graphene and lines joining Ir atoms along $\langle 112\rangle_{Ir}$ are continuous over steps. The latter is always the case on face centered cubic crystal (111) surfaces for all types of steps.
(32) Pan, Y.; Jiang, N.; Sun, J. T.; Shi, D. X.; Du, S. X.; Feng Liu; Gao, H.-J. *arXiv preprint* **2007**, arXiv:0709.2858v1.
(33) Qin, L. C.; Zhao, X.; Hirahara, K;, Miyamoto, Y.; Ando, Y.; Iijima, S. *Nature* **2000**, *408*, 50.

NL0728874